polymer

Structure of inhomogeneous polymer networks prepared from telechelic polybutadiene

Ivan Krakovský[a,*], Josef Pleštil[b], Josef Baldrian[b], Michael Wübbenhorst[c]

[a]*Department of Macromolecular Physics, Faculty of Mathematics and Physics, Charles University, V Holešovičkách 2, 180 00 Prague 8, Czech Republic*
[b]*Institute of Macromolecular Chemistry, Academy of Sciences of the Czech Republic, Heyrovský Sq. 2, 162 06 Prague 6, Czech Republic*
[c]*Department of Polymer Materials and Engineering, Faculty of Applied Sciences, Delft University of Technology, Julianalaan 136, 2628 BL Delft, The Netherlands*

Abstract

The structure and dynamics of segmented polyurethane networks prepared from poly(butadiene) diols (PBD) of different molecular weights M_n = 1200, 2160, 2650, 4690 and 10,300 g mol^{-1}, 4,4′-diphenylmethane diisocyanate (MDI) and poly(oxypropylene) triol (POPT) (M_n = 710 g mol^{-1}) have been investigated by dynamic mechanical analysis, dielectric relaxation spectroscopy, differential scanning calorimetry (DSC), small- and wide-angle X-ray scattering (SAXS and WAXS). Microphase separation on nanometre scale has been confirmed by SAXS in all networks. Except for the highest molecular weight of PBD, the networks consist of microdomains of similar size and composition dispersed in the soft phase of polybutadiene segments. Dielectric spectroscopy revealed the existence of three types of non-crystalline phases, each characterised by a well-developed dynamic glass transition. Absence of crystallinity has been proven by WAXS and DSC. © 2002 Elsevier Science Ltd. All rights reserved.

Keywords: Polyurethane network; Microphase separation; Dielectric spectroscopy

1. Introduction

Segmented polyurethanes represent a modern and versatile class of polymer materials because of their ability to form a wide range of well defined macromolecular architectures [1]. *Linear* segmented polyurethanes are usually prepared by end-linking reaction from a macrodiol of molecular weight of about 1000–5000 g mol^{-1}, a diisocyanate such as 4,4′-diphenylmethane diisocyanate and a low molecular weight diol, e.g. 1,4-butanediol as a chain extender [2]. They usually show a two-phase microphase separated structure consisting of the soft and hard phase of the order of a few hundreds angstroms or less [3].

In these polymers, the soft phase consists of flexible macrodiol chains and provides the polyurethane with high elasticity. The second hard phase is formed by the product of the reaction of diisocyanate molecules with the chain extender (short diols), which is usually glassy or even crystalline at room temperature or the temperature of usage.

In this way, segments of the hard phase act as physical junctions linking the chains of the soft phase to a thermoreversible network.

The driving force for the microphase separation is the thermodynamic incompatibility caused by a big difference in the polarity of the soft and hard segments, which can be quantified by their solubility parameters. Consequently, non-polar macrodiols like poly(butadiene) diol show a pronounced tendency to microphase separation. Furthermore, segmented polyurethanes based on poly(butadiene) diols are of increasing importance as they exhibit an excellent hydrolytic stability and superior mechanical properties [4–6].

If the functionality of the chain extender exceeds two, a *covalent network* containing a cross-linked hard phase will be obtained. Cross-links are expected to have two opposing effects on the structure and properties of polyurethane networks [7]. First, the presence of cross-links reduces the crystallinity of the hard phase, which results in a decline in the elastic modulus. Second, by virtue of a reduction of the chain mobility in the amorphous phase (increase in T_g), an increase in the elastic modulus and density of the network is often found.

---

* Corresponding author. Tel.: +420-2-21912369; fax: +420-2-21912350.
E-mail address: ivank@kmf.troja.mff.cuni.cz (I. Krakovský).
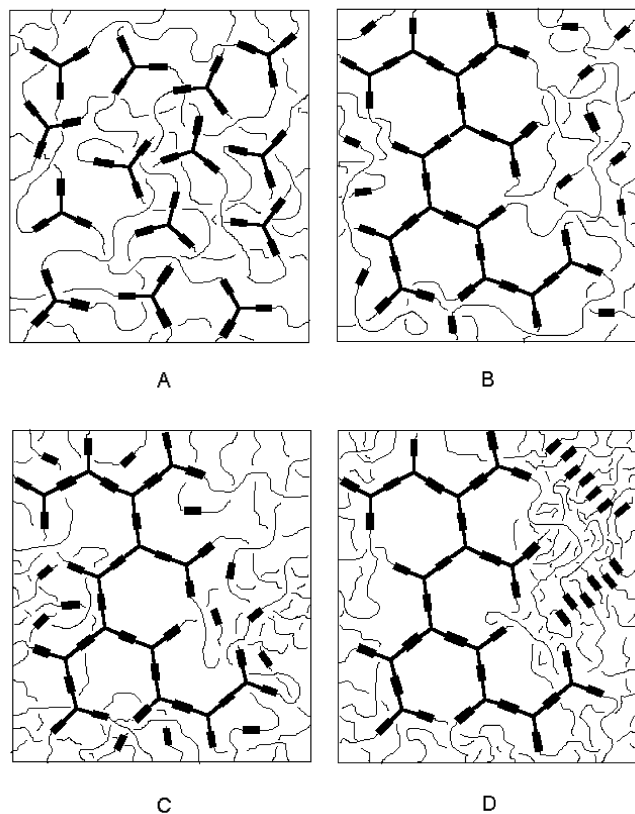
Fig. 1. Schematic view of polyurethane networks formed from the same (stoichiometric) monomeric mixture but showing a different degree of inhomogeneity: (a) homogeneous A (all components are distributed uniformly); (b) inhomogeneous B (triol molecules bridged with part of diisocyanate molecules form clusters, remaining diisocyanate molecules are distributed uniformly); (c) inhomogeneous C (the same as b, but remaining isocyanate molecules contribute to the triol clusters) and (d) inhomogeneous D (the same as b, but remaining diisocyanate molecules form separate clusters).

Cross-linking is also expected to have a restricting effect on the scale on which microphase separation in covalent networks is obtained. Networks of different topology and different degree of inhomogeneity can be formed at the same composition of the reaction system as it is shown in Fig. 1 for the case of a stoichiometric polyurethane network with molar ratio of the components: MACRODIOL/ DIISOCYANATE/TRIOL = 3:6:2. In the homogeneous polyurethane network (structure A, Fig. 1), all triol molecules are mutually separated by molecules of macrodiol and distributed uniformly in space. If triol molecules form clusters bridged by diisocyanate, an inhomogeneous network is realised. Remaining diisocyanate molecules participate in the formation of linear polyurethane chains from macrodiol and can be uniformly distributed in the soft phase (structure B, Fig. 1), become part of the hard phase involving triol molecules (structure C, Fig. 1), or form an independent hard phase of crystalline aggregates (structure D, Fig. 1).

In Ref. [8] the dependence of the structure of stoichiometric polyurethane networks prepared using poly-(butadiene) diol (PBD), 4,4′-diphenylmethane diisocyanate (MDI) and poly(oxypropylene) triol (POPT) on the content of the poly(butadiene) diol (with constant molecular weight) has been investigated. An inhomogeneous microphase separated structure with characteristic length of few tens angstroms has been revealed by small-angle X-ray scattering (SAXS).

In Ref. [9] the time evolution of inhomogeneous structure of linear and cross-linked polyurethanes has been studied by time-resolved SAXS. In the reaction between stoichiometric amounts of MDI and PBD which results to linear polyurethanes, the presence of the microdomains of reacting MDI molecules in early stages of the reaction has been observed. The interdomain distance was of the order of the root-mean-square end-to-end distance of PBD chains and did not change with reaction time. On the other hand, presence of POPT had a significant effect on the evolution of the microphase separated structure. Microdomains grow continuously with time, however, the process consists of two stages, before gelation of the system, the concentration of the microdomains decreases with time, while after gelation, it remains constant.

The aim of the present work is to investigate the influence of the chain length of the macrodiol PBD on the microphase separated structure of stoichiometric poly-urethane networks. This study refers to previous work on polyurethane networks based on PBD and POPT of a fixed molecular weight ($M_n = 5100$ and 710 g mol^{-1}, respect-ively). Phase separation effects will be addressed using X-ray scattering techniques as well as dynamic mechanical and dielectric relaxation spectroscopy (DRS).

2. Experimental

2.1. Materials

The networks were prepared using poly(butadiene) diols (synthesised at the Research Institute for Synthetic Rubber, Kaučuk Kralupy n.Vlt., Czech Republic) of different molecular weight; the properties of which are summarised in Table 1. The second component, POPT (ARCOL) has a molecular weight of $\bar{M}_n = 725 \text{ g mol}^{-1}$ and average functionality, $\bar{f}_n = 3$. Prior to the network synthesis, the polyols were dried under vacuum at 60 °C for one week. MDI was purified by vacuum distillation and recrystallised from dry n-heptane.

Networks were prepared by one-stage process. The initial concentration of reactive groups in the networks studied was kept at ratio

$[OH]_{PBD}/[NCO]_{MDI}/[OH]_{POPT} = 1 : 2 : 1$

After 15 min mixing in gaseous dry nitrogen at 60 °C, a small amount of the catalyst (0.001 wt% of dibutyltin dilaurate) was added and the reaction proceeded in rectangular shaped polypropylene moulds at 70 °C for

Table 1
Characteristics of poly(butadiene) diols and corresponding linear polyurethanes resulting from molar 1:1 reaction with MDI

Prepolymer (macrodiol)	$\bar{M}_n$ (g mol^{-1})	$\bar{M}_w/\bar{M}_n$	d_{PBD} (g cm^{-3})	$T_{g,PBD}^{DSC}$ (°C)	Linear polyurethane	
					$d_{PBD+MDI(1:1)}$ (g cm^{-3})	$T_{g,PBD+MDI(1:1)}^{DSC}$ (°C)
PBD 1	1200	1.2	0.908	-42	0.950	-26
PBD 2	2160	1.1	0.896	-43	0.931	-31
PBD 3	2650	1.1	0.894	-44	0.927	-37
PBD 4	4690	1.1	0.893	-52	0.901	-46
PBD 5	10,300	1.1	0.887	-54	0.909	-51

24 h. The samples prepared had a form of sheets about 1 mm in thickness. As a reference, a stoichiometric two-component polyurethane network (PUR 0) was also prepared from POPT and MDI at the same conditions.

Two-component linear polyurethanes were prepared from PBDs and MDI in smaller amounts at the same reaction conditions. Characteristic properties are given in Table 1.

The weight fractions of the sol, w_S, were determined from the weight loss after a three week extraction of the samples in toluene at room temperature. Densities of the polyurethanes were determined by the method of double weighting, in water and air. The densities of PBDs and POPT were determined using a pycnometric method.

2.2. Small-angle X-ray scattering

SAXS patterns were measured by Kratky camera with slit collimation using Cu K$_\alpha$ radiation with wavelength, $\lambda = 1.542$ Å. Intensities were transformed to smeared differential scattering cross-section (absolute scale), $d\tilde{\Sigma}/d\Omega(q)$, using the Lupolen sample as a secondary standard [10] and by using the relation

$$\frac{d\tilde{\Sigma}}{d\Omega}(q) = \frac{a\tilde{I}(q)}{\tilde{I}_L K_L Th},$$ (1)

where $\tilde{I}(q)$ is the measured intensity, $q = (4\pi/\lambda)\sin\theta$ is the magnitude of the scattering vector, 2θ is the scattering angle, a is the sample-detector distance. Further, T and h are transmission and thickness of the sample, respectively, K_L is the calibration constant and $\tilde{I}_L$ is the intensity of radiation scattered by the standard at $q = (2\pi/150)$ Å^{-1}.

The desmeared differential scattering cross-section, $d\Sigma/d\Omega(q)$ was calculated by means of the program ITR [11], based on the transformation

$$\frac{d\tilde{\Sigma}}{d\Omega}(q) = \frac{2}{K}\int_{-\infty}^{+\infty}\int_0^{+\infty} Q(x)P(y)\frac{d\Sigma}{d\Omega}\left[\sqrt{(q-x)^2+y^2}\right]dx\,dy,$$

where $K = 2\pi/(a\lambda)$ and $P(y)$, $Q(x)$ describe the length and width distribution of the primary beam intensity.

The mean square scattering density fluctuation, $\langle(\Delta\rho)^2\rangle$

was calculated by [12]

$$\langle(\Delta\rho)^2\rangle = \frac{K}{4\pi^2}\int_0^\infty q\frac{d\tilde{\Sigma}_c}{d\Omega}(q)dq,$$ (2)

where $d\tilde{\Sigma}_c/d\Omega(q)$ is the scattering cross-section corrected for the background scattering using the Vonk empirical formula [13]

$$\frac{d\tilde{\Sigma}_c}{d\Omega} = \frac{d\tilde{\Sigma}}{d\Omega} - (A_1 + A_2 q^m).$$ (3)

Here, A_1 and A_2 are empirical constants and best fits were obtained using $m = 1$.

The characteristic scale of inhomogeneity, D_B, was calculated from the position of scattering peak, q_{max}, on the desmeared SAXS profiles using the Bragg equation:

$$D_B = \frac{2\pi}{q_{max}}.$$ (4)

Further, we calculated the specific inner surface using the equation [14]:

$$\frac{S}{V} = \pi v_1 v_2 \frac{\lim_{q\to\infty} q^3 \frac{d\tilde{\Sigma}_c}{d\Omega}(q)}{\int_0^\infty q\frac{d\tilde{\Sigma}_c}{d\Omega}(q)dq}.$$ (5)

2.3. Wide-angle X-ray scattering

Wide-angle X-ray scattering (WAXS) experiments were carried out on HZG4A diffractometer (Freiberger Präzisionsmechanik, Germany) using Ni filtered Cu K$_\alpha$ radiation.

2.4. Dynamic mechanical analysis

Dynamic mechanical analysis (DMA) measurements on polyurethane networks were carried out using DMA 7e (Perkin–Elmer) in extension mode. All measurements were performed at a frequency of $f_{DMA} = 10$ Hz during heating at 5 °C min^{-1}.

2.5. Differential scanning calorimetry

Differential scanning calorimetry (DSC) measurements

Table 2
Characteristics of polyurethane networks

Sample	Appearance	w_S	d_{netw} (g cm^{-3})	$\langle(\Delta\rho)^2\rangle$ ($\times 10^{-19}$ cm^{-4})	D_B (Å)	$T_{g,1}^{DSC}$ (°C)	$T_{g,2}^{DSC}$ (°C)	T_g^{DMA} (°C)
PUR 0	Clear	<0.01	1.146	–	–	30	–	37
PUR 1	Clear	<0.01	1.011	9.4 ± 0.9	61	−15	12	20
PUR 2	Clear	<0.01	0.974	8.0 ± 0.8	81	−27	8	5
PUR 3	Clear	<0.01	0.964	7.8 ± 0.8	88	−30	4	−14
PUR 4	Clear	0.03	0.946	5.2 ± 0.5	100	−42	–	−35
PUR 5	Opaque	0.23	0.930	4 ± 1	100	−45	–	−37

were performed using a Pyris 1 DSC from Perkin–Elmer. Samples with a typical mass of 40 mg were examined both in heating and cooling with a rate of ± 10 °C min^{-1}. The purge gas was helium. Glass transition temperatures were determined by means of the inflexion points on the calorigrams from the second heating runs.

2.6. Dielectric spectroscopy

Dielectric measurements were performed in the frequency range from 10^{-2} to 10^6 Hz using a combination of two dielectric analysers covering partially overlapping frequency ranges: (a) a frequency response analyser (Schlumberger 1260) equipped with a custom made dielectric interface (TNO) for frequencies between 10^{-2} and 10^4 Hz, and (b) a Hewlett/Packard 4284A precision LCR-meter for frequencies between 10^2 and 10^6 Hz.

For the dielectric measurements, circular samples were cut from the dried polyurethane sheets and metallised on both sides (20 mm diameter) by sputtering with Au. Subsequently, the samples were placed in a cryostat (Novocontrol), the temperature of which was controlled with nitrogen gas with a stability better than 0.05 K. More details about the experimental set-up can be found in Ref. [15].

3. Results and discussion

The characteristics of the poly(butadiene) diols and the resulting linear stoichiometric polyurethanes are listed in Table 1. Glass transition temperatures of PBDs decrease with increasing molecular weight of the polymer. This tendency is opposite to the usual behaviour of linear polymers described by the Flory–Fox equation and is a direct consequence of the decrease in chains mobility due to the formation of associates of the hydroxy endgroups [16] acting as physical cross-links. The same trend for linear polyurethanes can be attributed to the decrease of chains mobility due to hydrogen bonding between urethane groups.

Table 2 presents some characteristics of the polyurethane networks. Except for sample PUR 5, all samples were clear and low weight fractions of sol were obtained. These results confirm that both high conversions of the reactive groups and no macrophase separation have been obtained.

Fig. 2 shows the smeared SAXS scattering profiles. The two-component network does not show any sign of inhomogeneity. In contrast, all three-component networks show an increased scattering at small angles. Except for one, all scattering profiles in the Porod region scale as q^{-n} with n close to 3. In particular $n = 3$ is typical for microphase separated structure with well-developed interphase boundaries. Consequently, we may exclude the scenario represented by the structure A in Fig. 1(a) in the following considerations.

Fig. 3 shows the corresponding desmeared SAXS profiles. Peaks were obtained for all microphase separated samples. However, only the main peaks with highest q values are meaningful, as the peaks at smaller angles represents artefacts arising from deconvolution. The position of the main peaks was used in the calculation of the values of the characteristic distance of inhomogeneity, D_B, given in Table 2. Except for the last sample, these distances scale with the molecular weight of PBD as $M_n^{1/2}$.

Scattering halos present in WAXS patterns (Fig. 4) do not provide any evidence of crystallinity in all three-component networks. Consequently, the scenario according to Fig. 1(d) can also be excluded from further considerations.

In order to decide between the remaining structures B and C, we have calculated volume fractions, specific masses and expected mean square scattering densities, $\langle(\Delta\rho)^2\rangle$.
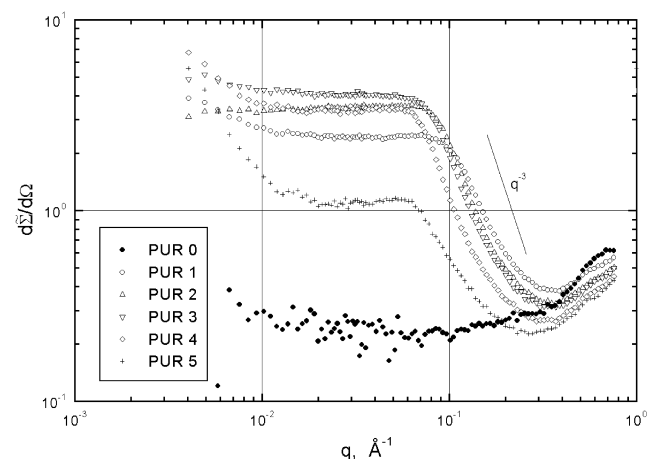
Fig. 2. SAXS patterns of polyurethane networks (smeared differential cross-section, $d\tilde{\Sigma}/d\Omega(q)$ vs. magnitude of the scattering vector q).
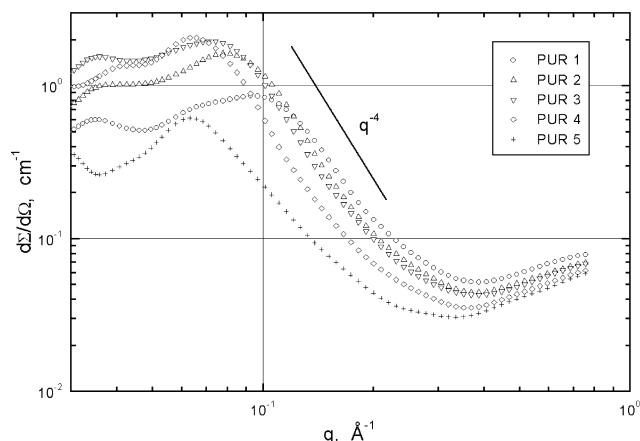
Fig. 3. Desmeared SAXS patterns of polyurethane networks (desmeared differential cross-section, $d\Sigma/d\Omega(q)$ vs. magnitude of the scattering vector q).

Mean square scattering densities were calculated using

$$\langle(\Delta\rho)^2\rangle = v_1 v_2(\rho_1 - \rho_2)^2, \tag{6}$$

where v_1 and v_2 are volume fractions of the two different phases. The scattering density of the material, ρ is related to its specific mass, d, by

$$\rho = \frac{\sum_i Z_i}{\sum_i M_i} N_A bd, \tag{7}$$

where Z_i and M_i are atomic numbers and relative atomic masses of the elements the material consists of, $b = 2.82 \times 10^{-15}$ m being the scattering amplitude for a single electron according to Thomson's formula, N_A is the Avogadro constant. Volume additivity was assumed in our calculations. The results are summarised in Tables 3 (structure B) and 4 (structure C), respectively.

It can be seen that for the samples, PUR 1–PUR 3, the experimental scattering densities (Table 2) are in fair agreement with those calculated for the structure C. The
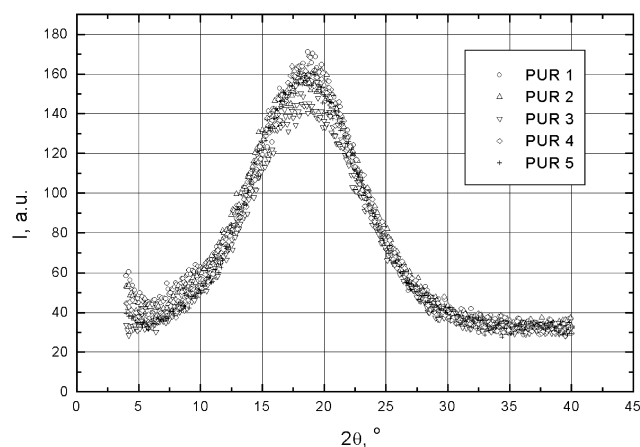
experimental value obtained for sample PUR 4 lies in between the predicted value for structure B and C, respectively.

Volume fractions of the minor phase in the samples PUR 1–PUR 4 calculated for structure C ($v_2 = 0.163$–0.336, see Table 4) lie in the region where a spherical shape of the microdomains can be expected. The absence of the side maxima in the desmeared SAXS patterns and the values of the slopes of the patterns in the Porod region close to -4 (Fig. 4) lead us to the conclusion that the size of the microdomains is rather widely distributed. Although the accuracy of the experimental data did not allow the quantitative determination of such a distribution, we are able to obtain the mean radius of the microdomains, $\bar{R}$, from the specific inner surface according to Eq. (8):

$$\bar{R} = \frac{3v_2}{S/V}. \tag{8}$$

Interestingly, the mean radii of microdomains for the samples PUR 1–PUR 4 (Table 4) attain values of 17–18 Å and *do not change* with molecular weight of PBD. This result is in agreement with our previous results ($\bar{R} \approx 19$ Å for the three-component network prepared using PBD of molecular weight ≈ 5200 g mol^{-1}, cf. Ref. [8]) and it is also confirmed by the plot of smeared SAXS patterns normalised by volume fractions of minor phase which roughly follow the same line in the Porod region (Fig. 5).

Deviations in SAXS patterns obtained for the PUR 5 sample, prepared using longest polybutadiene can likely be attributed to the upcoming role of entanglement formation. The molecular weight of PBD 5 ($\bar{M}_n = 10,300$, see Table 1) exceeds the critical molecular weight for entanglement formation estimated for polybutadiene ($M_c \approx 5900$ g mol^{-1} for 1,4-polybutadiene, based on the viscosimetry, cf. Ref. [17]). An increased viscosity of the reaction system in early stages of the network formation slows down the rate of microphase separation. Consequently, higher amounts of

Fig. 4. WAXS patterns of polyurethane networks (scattering intensity I vs. scattering angle θ).
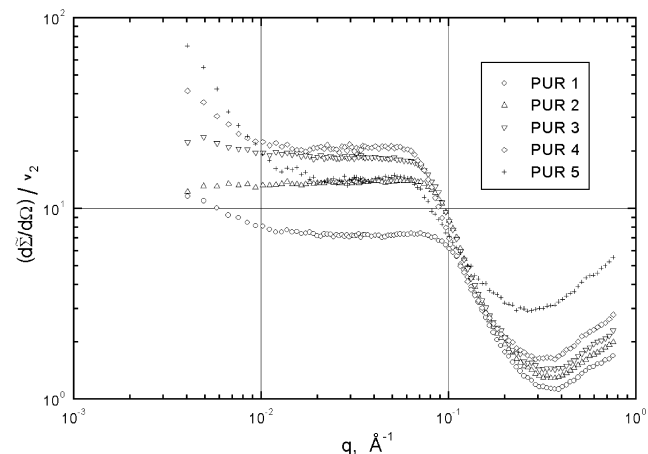
Fig. 5. Smeared SAXS patterns of polyurethane networks normalised by the volume fraction of minor phase, v_2, calculated assuming the structure C from Fig. 1(c).

Table 3
Calculated network parameters assuming structure B (Fig. 1(b))

Sample	d_1 (g cm^{-3})	d_2 (g cm^{-3})	v_1	v_2	d_{netw} (g cm^{-3})	$\langle(\Delta\rho)^2\rangle$ ($\times 10^{-19}$ cm^{-4})
PUR 1	0.950	1.140	0.744	0.256	0.999	4.9
PUR 2	0.931	1.140	0.807	0.193	0.971	4.8
PUR 3	0.927	1.140	0.833	0.167	0.963	4.4
PUR 4	0.901	1.140	0.877	0.123	0.930	4.3
PUR 5	0.909	1.140	0.940	0.060	0.923	2.1

Table 4
Calculated network parameters assuming structure C (Fig. 1(c))

Sample	d_1 (g cm^{-3})	d_2 (g cm^{-3})	v_1	v_2	d_{netw} (g cm^{-3})	$\langle(\Delta\rho)^2\rangle$ ($\times 10^{-19}$ cm^{-4})	$\bar{R}$ (Å)
PUR 1	0.887	1.155	0.664	0.336	0.991	10.2	18
PUR 2	0.887	1.155	0.747	0.253	0.962	8.7	17
PUR 3	0.887	1.155	0.781	0.219	0.951	7.8	18
PUR 4	0.887	1.155	0.837	0.163	0.936	6.3	17
PUR 5	0.887	1.155	0.922	0.078	0.908	3.3	–

MDI remain part of the linear polyurethane chains and the network is more homogeneous.

3.1. Effects of the network structure on the dynamic glass transition

DSC thermograms of all polyurethane samples are shown in Fig. 6. In all cases, a calorimetric glass transition was found at low temperatures ($T_{g,1}$), indicated by a step in the endothermic heat flow. Apart from this, samples with a higher concentration of microdomains reveal a second transition ($T_{g,2}$). The glass transition temperatures are given in Table 2. The lower transition temperature shifts with the composition, being between the glass transition of the PBD with highest molecular weight and that of the two-component network (PUR 0). The high-temperature transition $T_{g,2}$ is much broader than the $T_{g,1}$ and corresponds to the minor phase. $T_{g,2}$ also shifts with composition and

cannot be determined unambiguously any more for the two lowest microdomain concentrations. No melting or crystallisation peak was found by DSC, which is in full agreement with the WAXS observation.

Fig. 7 shows the temperature dependence of the mechanical storage modulus and loss tangent for the networks at the temperature range -100 to $+150\,^{\circ}$C. Unlike DSC, only one distinct glass transition was obtained for each sample. Owing to the measurement frequency of the DMA experiment ($f_{DMA} = 10$ Hz) being much higher than the equivalent frequency of the DSC runs (typically

Fig. 6. DSC traces (2nd heating at 10 °C min^{-1}) for polyurethane networks. Arrows indicate glass transitions temperatures $T_{g,1}$ and $T_{g,2}$ determined from inflexion points.
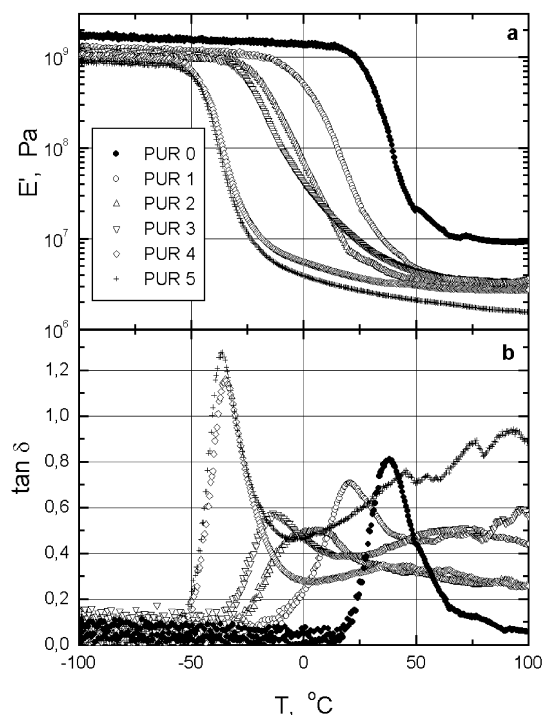
Fig. 7. The temperature dependence of the storage Young modulus, E' (a) and tangent of mechanical losses, tan δ (b) at $f_{DMA} = 10$ Hz.

10^{-3} Hz), DMA loss peaks appear systematically shifted towards higher temperatures compared to the calorimetric glass transition temperatures.

On search for further manifestations of the phase separated morphology in the dynamic properties we have used DRS operating in a wide frequency range (10^{-1}–10^{6} Hz). Since DRS is specifically sensitive for molecular motions of molecular dipoles, i.e. polar groups (here mainly urethane groups), DRS focuses particularly on the relaxation processes involving the urethane groups.

Fig. 8 shows the temperature dependences of dielectric constant ε' and dielectric loss ε'' at the frequency 7 Hz. Let us first discuss the permittivity which is compared for all polyurethane networks as shown in Fig. 8(a). Clearly one sees a continuous decrease in the relaxation strength, roughly proportional to the maximum in $\varepsilon'(T)$, with increasing length of the macrodiol. Since PBD is practically unpolar, an increasing molecular mass of PBD leads to an
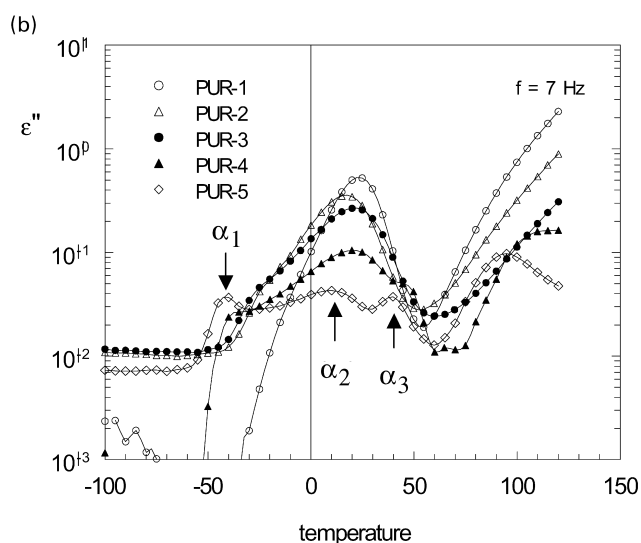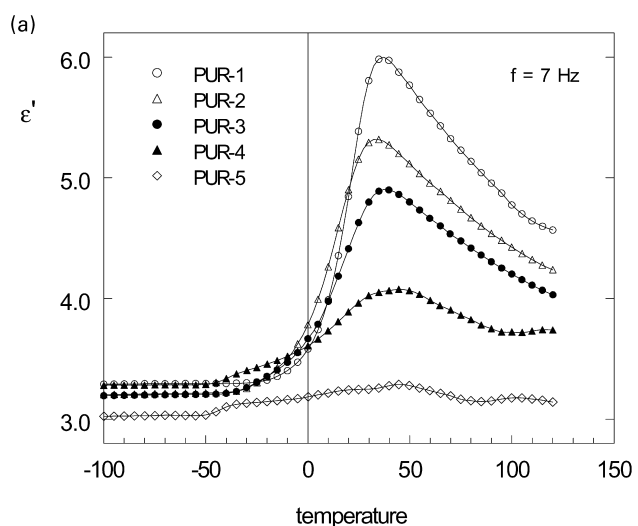
increasing volume fraction of PBD and thus to a decreasing concentration of polar (urethane groups) in the PUR network.

Fig. 8(b) shows the dielectric loss at the same frequency, which reveals interesting details about the dynamic glass transition. Upon increasing the molecular weight of PBD, the loss peak shows a gradual change from a single loss peak in $\varepsilon''(T)$ to a split loss peak, consisting of three well distinct peak maxima. This peak splitting persists over a wide frequency range (Fig. 9) indicating that for high molecular masses of PBD three network fractions are present, each characterised by an individual glass transition. Having in mind that the calorimetric glass transition of the PBD phase is in the order of $-50\ °C$, we can assign the α_1 process to the T_g of a linear PBD + MDI fraction, whereas the α_3 process refers to the dynamics of the dense network fraction mainly involving the POPT/MDI fraction. In contrast to the α_1 and α_3 relaxations, the third, intermediate α_2 process shows a strong broadening which supports the idea that the α_2 process reflects the dynamics of a transition region, i.e. a mixed phase containing both diol and triol-groups as shown in Fig. 1(c).

Another indication of increasing network heterogeneity is the decrease in $\varepsilon''(T)$ at high temperatures due to a decreasing overall conductivity; this is accompanied with the appearance of interfacial polarisation (IF, cf. Fig. 9), most likely caused by charge blocking at the less mobile and thus less conducting POPT/PBD domains.

The detection of phase specific glass transitions by dielectric spectroscopy provides finally a *lower limit* for the size of the dynamically distinct region, given by the length of cooperativity being $20-30\ Å$ close to T_g. This length scale is in fair agreement with the results deduced from SAXS experiments.

4. Conclusions

Segmented polyurethane networks were prepared by

Fig. 8. Temperature dependence of the permittivity ε' (a) and dielectric loss ε'' (b) at $f = 7$ Hz for samples PUR 1–PUR 5.
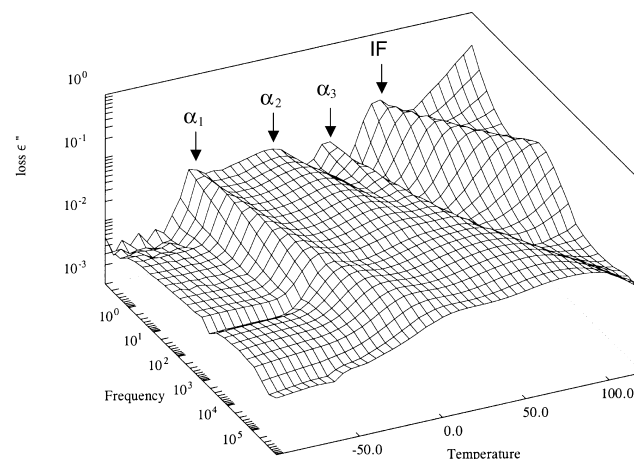
Fig. 9. 3D representation of the dielectric loss $\varepsilon''(f, T)$ for sample PUR 5.

end-linking reaction between poly(butadiene) diol, 4,4'-diphenylmethane diisocyanate and poly(oxypropylene) triol, which resulted in microphase separated structures as confirmed by SAXS. In this study, the particular influence of the length of the poly(butadiene) diol on the network structure and its dynamics was studied systematically.

Except for the poly(butadiene) diol of the highest molecular weight, all networks consist of the matrix of polybutadiene segments (soft phase) in which microdomains of the similar size and composition are dispersed at different concentrations. All materials were found to be fully amorphous as verified by WAXS and DSC.

A low-temperature glass transition, indicating the existence of a phase separated *soft phase* consisting of polybutadiene segments has been found in all three-component networks both by calorimetric and dynamic mechanical experiments. A second glass transition at higher temperatures, reflecting the dynamic properties of the hard phase, was observed only by DSC in samples with a high concentration of microdomains. Both transitions shift with molecular weight of PBD giving another evidence for a rather fine scale of microphase separation.

DRS provided additional evidence for the tendency of the polyurethane networks to become gradually inhomogeneous upon increasing the molecular weight of the polybutadiene macrodiols. Whereas in networks containing short PBDs only a single structural relaxation (α process) was found, indicating a dynamically homogeneous system on the length scale of a few nanometre, three well distinct glass transition processes ($\alpha_1 - \alpha_3$) implying the presence of *three distinct phases* were found for high molecular weight macrodiols.

In line with the results from DSC and DMA, the low-temperature process (α_1) was clearly assigned to the soft network fraction build-up from MDI and PBD, while the high-temperature relaxation process (α_3) refers to the dense (hard) polyurethane network fraction formed from POPT and MDI. An intermediate third relaxation process (α_2) most likely indicates the existence of a mixed phase containing segments from both, linear and cross-linked polyurethane. This idea is supported by the extreme peak width, indicating a broad distribution in relaxation times caused by the intrinsic heterogeneity of this mixed phase.

Deviations from the trend sketched earlier, found for the sample containing the longest PBD in SAXS results, are probably caused by increased viscosity due to the presence of entanglements in early stages of the network formation process.

References

[1] Oertel G. Polyurethane handbook. New York: Hanser Publishers; 1985.
[2] Macosko CW. Fundamentals of reaction injection molding. New York: Hanser Publishers; 1988.
[3] Chen CHY, Briber RM, Thomas EL, Xu M, MacKnight WJ. Polymer 1983;24:1333.
[4] Reagan PR, Teo HH, Booth C, Cunli AV, Hudd AL. Br Polym J 1985; 17:22.
[5] Ninan KN, Balagagadharan VP, Catherine KB. Polym J 1991;32:628.
[6] Minoura Y, Okamoto H, Matsuo T. J Appl Polym Sci 1978;22:817.
[7] Petrovič Z, Javni I, Divjakovič V. J Polym Sci 1998;36:221.
[8] Krakovský I, Bubeníková Z, Urakawa H, Kajiwara K. Polymer 1997; 38:3637.
[9] Krakovský I, Urakawa H, Kajiwara K. Polymer 1997;38:3644.
[10] Kratky O, Pilz J, Schmidt PJ. J Colloid Interf Sci 1966;61:24.
[11] Glatter O, Gruber K. J Appl Crystallogr 1993;26:512.
[12] Pleštil J, Hlavatá D. Polymer 1988;29:2216.
[13] Vonk CG. J Appl Crystallogr 1973;6:81.
[14] Kratky O. Prog Biophys 1963;13:105.
[15] Mertens IJA, Wübbenhorst M, Oosterbaan WD, Jenneskens LW, van Turnhout J. Macromolecules 1999;32:3314.
[16] Krakovský I, Trchová M, Hanyková L, Demchenko Y. In preparation.
[17] Ferry JD. Viscoelastic properties of polymers. New York: Wiley; 1980.